Volume 1 | Number 1 | Jan 2013 | Pages 1–100

Journal of
Materials Chemistry A

Materials for energy and sustainability
www.rsc.org/materialsA

ROYAL SOCIETY
OF CHEMISTRY

ROYAL SOCIETY
OF CHEMISTRY

www.rsc.org/materialsA

Journal Name

COMMUNICATION

ROYAL SOCIETY OF CHEMISTRY

Fast capture of methyl-dyes over hierarchical amino-Co$_{0.3}$Ni$_{0.7}$Fe$_2$O$_4$@SiO$_2$ nanofibrous membrane

Zhigao Zhu[a], Guihua Li[a], Gaofeng Zeng[a], *, Xinqing Chen[a], Deng Hu[a], Yanfeng Zhang[a, b],*, Yuhan Sun[a, b]

Flexible polydopamine-Co$_{0.3}$Ni$_{0.7}$Fe$_2$O$_4$@SiO$_2$ NFMs with hierarchical structure and strong magnetism were prepared by gelation, calcination and dopamine self-polymerization on electrospun SiO$_2$ NFMs. The resulting membranes displayed a short response time (10 min/80%), high adsorption capacity and excellent adsorption affinity (97%) for the methyl orange capture.

Organic dyes have been extensively used in the textile industry for decades. However, the large amount of colored wastewater generated during dying process caused serious pollution/damage to the environment, which requires appropriate treatment technologies for efficient removal of dyestuffs from waste water[1]. Among the numerous techniques of dye removal, adsorption is the procedure of choice to balance the water pollution pressure by capturing the contaminants from wastewater because it offers advantages of high efficiency, simple processing, and zero secondary pollution[2]. For the treatment of organic dyes such as Congo red (CR), methylene blue (MB), methylene orange (MO) and malachite green (MG), a large number of adsorbents have been proposed, including activated carbon, clays, silica and the new rising magnetic nanoparticles (NPs)[3-6]. Large surface area is a prerequisite for a superior adsorbent because the adsorption capacity normally depends on the effective surface area. Such appeal can be achieved by creating inner micropores or narrowing the adsorbent itself to nanoscale e.g. nanoparticle (NPs)[7-9]. For the former approach, the adsorption capacity is limited by the mass transfer through the micro-channels[10, 11]. On the contrary, the adsorbent surface area can be fully utilized in the case of NPs due to its high dispersibility[12]. However, the recovery of nanoparticle adsorbents is difficult. Moreover, the residual NPs would cause the secondary pollution to water[13]. Therefore, it is desirable to design a sorbent with high and easy accessible surface area with simple recovery.

Constructing the adsorbents with hierarchical structure, which contains well-organized macro-/meso- and micro-pores, is one of the efficient methods to provide large surface area as well as unobstructed diffusion pathway. Among various approaches supporting nanoparticles on macro-/meso-pore templates is a feasible strategy. Silica nanofiber membrane (NFM) prepared by electrospinning is an ideal candidate template owing to its robust mechanical properties, low density, high surface area and excellent flexibility[14-18]. Si *et al.* immobilized γ-Fe$_2$O$_3$ NPs onto the surface of SiO$_2$ NFM and obtained a quick response time (15 min/89 %) to MB adsorption[19]. The positively charged metal oxide NPs has strong affinity towards negatively charged anionic dye. Miao *et al.* also successfully fabricated hierarchical SiO$_2$@γ-AlOOH (Boehmite) core/sheath fibers by hydrothermal synthesis and demonstrated an enhanced scavenging ability to Congo red and microorganism[20]. However, to access the NFM based adsorbents with high particle adhesive strength, uniform particle distribution and easy recovery are still big challenges unresolved by far.
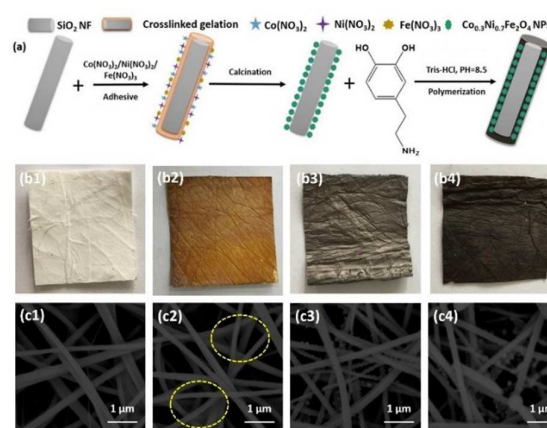
a. *CAS key Laboratory of Low-carbon Conversion Science and Engineering, Shanghai Advanced Research Institute, Chinese Academy of Sciences, Shanghai, 201210, China. E-mail: zengqf@sari.ac.cn; zhangyf@sari.ac.cn; Fax/Tel: +86 21 20350958*
b. *School of Physical Science and Technology, Shanghai Tech University, Shanghai 201210, China.*
Electronic Supplementary Information (ESI) available: [Experimental details, SEM, XRD, BET, XPS and adsorption kinetics results]. See DOI: 10.1039/x0xx00000x

Fig. 1 (a) Schematic of the synthesis procedure of PDA-Co$_{0.3}$Ni$_{0.7}$Fe$_2$O$_4$@SiO$_2$ NFMs. Optical photographs / SEM views of (b1)/(c1) SiO$_2$ NFMs, (b2)/(c2) gelation/SiO$_2$ NFMs, (b3)/(c3) gelation/SiO$_2$ NFMs after calcination at 700 °C in N$_2$ and (b4)/(c4) PDA-Co$_{0.3}$Ni$_{0.7}$Fe$_2$O$_4$@SiO$_2$ NFMs.

In this communication, we designed and fabricated flexible polydopamine-$Co_{0.3}Ni_{0.7}Fe_2O_4$@SiO_2 NFMs with hierarchical structure and high magnetism by decorating magnetic NPs and ultrathin amino coating layer on electrospun SiO_2 nanofiber membrane in sequence, and successfully applied them for efficient capture of MO and MB. The positively charged metal oxide NPs provide affinity towards anionic dyes as well as extra surface area for high adsorption capacity. The polydopamine coating not only protects the NPs from leaching, but also provides adsorption selectivity towards organic dyes due to its hydrophobic nature. This hybrid adsorbent has multiple advantages of high and accessible surface area, high affinity towards anionic dyes, great stability and flexibility as well as easy recovery.

The synthesis procedure was showed in Fig. 1a. The SiO_2 NFM was fabricated by calcination of electrospun tetraethyl orthosilicalite/poly (vinyl alcohol) hybrid nanofibers (Fig.1 b1&c1). Then the SiO_2 NFM was dipped in a mixture of 1 wt% paper-adhesive aqueous and a 4 wt% $Fe(NO_3)_3$ / $Co(NO_3)_2$ / $Ni(NO_3)_2$ solution in sequence, followed by heating at 50 ^{o}C for 1 h to form a gel layer on the fiber surface (Fig.1 b2&c2). The former conditions for NPs formation were screened out from the range of 0.5-2.0 wt% adhesive and 1.0-8.0 wt% metal ion concentration. Under the optimized conditions, the morphology of NFM was well protected and agglomeration of NPs was successfully avoided (Fig. S1 & S2). The molar ratio of Co^{2+}, Ni^{2+} and Fe^{3+} were fixed at 0.3: 0.7: 2.0 to achieve the best magnetism[21]. After gelation, the membrane was calcined at 700 ^{o}C in N_2 to generate mixed oxides of $Co_{0.3}Ni_{0.7}Fe_2O_4$@SiO_2 NFM (Fig. 1 b3&c3). Finally, the prepared membrane was immersed in dopamine solution（2 mg/ml in 10 mM Tris buffer, pH=8.5 ） and followed by a self-polymerization process under alkaline condition (Fig.1 b4&c4). See more experimental details in ESI. The as-prepared SiO_2 nanofibres are ~300 nm in diameter. During these gelation, calcination and polymerization treatments, no visible changes were observed regarding the fibre morphology and size (Fig. c1-4). The flexibility of the final membrane was well preserved while the colour changed from white to black (Fig. b1-4 & S3a).
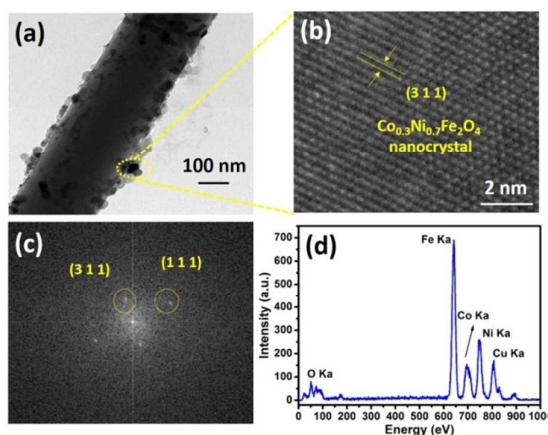

Fig. 2 (a) TEM image of signal PDA-$Co_{0.3}Ni_{0.7}Fe_2O_4$@SiO_2 nanofiber, (b) HRTEM image of the $Co_{0.3}Ni_{0.7}Fe_2O_4$ nanocrystal in (3 1 1) orientation, (c) SEAD pattern of $Co_{0.3}Ni_{0.7}Fe_2O_4$ NPs and (d) EDS measurement of $Co_{0.3}Ni_{0.7}Fe_2O_4$ nanocrystal.

As shown in Fig. 2(a), nanoparticles with size range 20-70 nm were homogeneously distributed on the SiO_2 fiber surface without obvious agglomeration. At low magnitude, the porous structure of NFM was well retained after the attaching of nano-particles (Fig. 1c). EDS mapping in Fig. S4 manifested the uniform distribution of Fe/Co/Ni on the fiber surface. The dispersion of metal oxide NPs is much better than that prepared by direct hydrothermal synthesis method[22]. It means that the precursors Co^{2+}, Ni^{2+} and Fe^{3+} were well inlayed in the glue during the gelation step, which prevented the sintering / agglomeration of nano-particles in the following calcination treatment (Fig. 1c2-4). EDS result showed an atomic ratio of 3.6Fe: 1.4Ni: 0.6Co, which is very close to the ratio of dip-coating solution (2Fe:0.7Ni:0.3Co) (Fig. 2d & S5). HRTEM analysis of the hybrid magnetic $Co_{0.3}Ni_{0.7}Fe_2O_4$ NPs reveals an interplane distance of 0.25 nm for (3 1 1) plane of $Co_{0.3}Ni_{0.7}Fe_2O_4$ (Fig. 2b). The selected area electron diffraction (SAED) patterns of $Co_{0.3}Ni_{0.7}Fe_2O_4$ NPs shows spotty ring patterns (3 1 1) and (1 1 1) without any additional diffraction spots, which reflects the complete crystalline of NPs (Fig. 2c). The flexibility and magnetism of PDA-$Co_{0.3}Ni_{0.7}Fe_2O_4$@SiO_2 NFMs was demonstrated directly in Fig. S3. Benefit from the high entanglement of silica fibers, the resultant NFM can be easily rolled up without cracking. NFMs could be easily caught by a magnet. The mechanical stability as well as the magnetism would provide the practical usability and easy recovery in the water purification[23, 24].
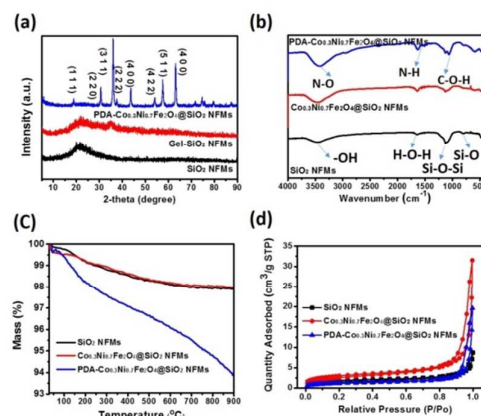

Fig. 3 (a) XRD patterns, (b) FT-IR spectra, (c) TG curves, and (d) N_2 adsorption – desorption isotherms of NFMs.

The original and modified NFMs at different stages were characterized by XRD, FT-IR, TG and N_2 adsorption (as shown in Fig. 3). Based on the XRD patterns in Fig. 3a & Fig. S6, the original SiO_2 NMF was amorphous before and after gelation treatment. With the attaching of Co^{2+}, Ni^{2+} and Fe^{3+} oxides, the peaks appeared at 2θ of 17.80^o (1 1 1), 29.98^o (2 2 0), 35.29 ^{o} (3 1 1), 36.95^o (2 2 2), 42.91^o (4 0 0), 53.30^o (4 2 2), 56.80^o (5 1 1) and 62.35^o (4 0 0), which could be attributed to the $Co_{0.3}Ni_{0.7}Fe_2O_4$ phase (JCPDS, no. 53-125)[21]. The polymerization of dopamine was proved by FT-IR. For the original SiO_2 NFM, the adsorption band of 3449, 1637, 1095 and 799 cm^{-1} were assigned to –OH, H-O-H (from water vapor),

Si-O-Si and Si-O, respectively. In the case of dopamine modified $Co_{0.3}Ni_{0.7}Fe_2O_4@SiO_2$ NFM, the adsorption band of 3425, 1507 and 1130 cm^{-1} were assigned to the stretching of phenolic vibration of O-H and N-H, amide group N-H and C-O-H stretching vibration, respectively (Fig. 3b)[25,26]. The other relative weak peaks at around 430, 668 and 567cm^{-1} come from Ni-O, Co-O and Fe-O of the inorganic NPs, respectively[27-29]. The weight percentage of dopamine coating was derived from the weight loss in heat treatment. Both of original SiO_2 NFM and the $Co_{0.3}Ni_{0.7}Fe_2O_4@SiO_2$ NFM weight loss were about 1.8 wt.% at 900 ^{o}C in air, while polydopamine coated $Co_{0.3}Ni_{0.7}Fe_2O_4@SiO_2$ NFM shows a weight loss about 6.2 wt.% , indicating 4.4 wt.% of PDA was loaded. The interaction between NPs and the SiO_2 NFM was measured by XPS. The peak with the binding energy of 101.7 eV was assigned to the bond of Si-O-Metal (Fe) (Fig. S7a), which indicated the strong bonding between NPs and SiO_2 fiber support were formed during the high temperature calcination[30]. By contrast, the Si-O-Fe peak was indiscernible from the Si2p spectra of the physical mixed SiO_2 fibers and Fe/Co/Ni oxides (Fig. S7b). The strong adhesion force between NPs and SiO_2 NFM was also supported by the TEM result in Fig. 2a because most NPs survived the grinding and ultrasonic treatments in the preparation of TEM samples. Of course, the PDA coating layer further protects the NPs from leaching. $Co_{0.3}Ni_{0.7}Fe_2O_4$ NPs endowed the pristine SiO_2 NFM with hierarchical rough structure, thus significantly improved the porosity and effective surface area. The N_2 adsorption-desorption isotherms and the calculated pore size distribution of SiO_2, $Co_{0.3}Ni_{0.7}Fe_2O_4@SiO_2$ and PDA-$Co_{0.3}Ni_{0.7}Fe_2O_4@SiO_2$ NFMs are shown in Fig. 3(d) and Fig. S8. All isotherms are typical- IV isotherm with N_2 hysteresis loop, which indicated the presence of mesopores (Fig. 3d). The narrow H 1 hysteresis loop in the region of P/P$_0$>0.9 indicated that the mesopores are open with a capillary condensation phenomenon. The surface areas of SiO_2, $Co_{0.3}Ni_{0.7}Fe_2O_4@SiO_2$ and PDA-$Co_{0.3}Ni_{0.7}Fe_2O_4@SiO_2$ NFMs are 5.8, 32.4 and 23.2 m^2/g, respectively. Attaching $Co_{0.3}Ni_{0.7}Fe_2O_4$ NPs onto the fiber surface significantly increase the surface area from 5.8 to 32.4 m^2/g, which is the result of extra rugged surface from the tiny NPs. However, the surface area exhibited substantial decrease to 23.2 m^2/g after dopamine coating, which might be attributed to smoothing effect. The pore size distribution shown in Fig. S8 indicated that the $Co_{0.3}Ni_{0.7}Fe_2O_4$ NPs@SiO_2 had a typical mesoporous feature with an average pore size of 50 nm, which comes from the stacking of SiO_2 nanofibers, and the final NFM with a pore volume of 0.06 cm^3/g.

The adsorption performance of PDA-$Co_{0.3}Ni_{0.7}Fe_2O_4@SiO_2$ NFMs (ca. 5 mg) was measured in a 30 mL of 20 ppm MO or MB solution by a UV-vis spectrometer. The adsorption capacity was calculated using the following equation:

$$q_t = \frac{(C_0 - C_t) \times V}{m}$$

Where q_t (mg/g) is the absorption capacity at time t; C_0 (mg/L) and C_t (mg/L) are the initial concentration and the concentration at time t, respectively; V (L) is the volume of the

solution and m (g) is the mass of the membrane. For the purpose of comparison, original SiO_2 NFM and $Co_{0.3}Ni_{0.7}Fe_2O_4@SiO_2$ NFM were also tested under the same conditions. Pure silica fiber membrane has almost zero adsorption capacity for MO and MB even after a long equilibrium time of 100 min, whereas the equilibrium adsorption capacities of $Co_{0.3}Ni_{0.7}Fe_2O_4@SiO_2$ NFM for MO and MB were increased to ca. 80.0 and 71.1 mg/g, respectively (Fig. 4a & c). It suggested that the mixed oxide of Fe/Co/Ni nanoparticles have the similar adsorption performance to single phase Fe_2O_3 NPs[31], which was contributed by the enhanced surface area, electrostatic attraction and low diffusion resistance. For the PDA modified $Co_{0.3}Ni_{0.7}Fe_2O_4$ @SiO_2 NFM, the equilibrium adsorption capacities of MO and MB were 116.2 mg/g and 107.5 mg/g, respectively, which were improved by 45.3 and 51.4 % comparing with $Co_{0.3}Ni_{0.7}Fe_2O_4@SiO_2$ NFM (Fig. 4a&c). PDA coating can generate a stable polymer layer on the fibers and NPs surface, which has strong electrostatic attraction, hydrogen bonding and π-π stacking interactions due to the presence of aromatic rings[32, 33]. On the other hand, the nanoparticles were also considered as the key role for the high adsorption capacity. Because the adsorption capacities of PDA@SiO_2 NFM for MO and MB were only 53.6 and 47.3 mg / g, respectively, which are more than 50% less than those of PDA-$Co_{0.3}Ni_{0.7}Fe_2O_4@SiO_2$ NFMs. It demonstrated that the extra surface area and hierarchical structure provided by NPs greatly contributed to the adsorption capacity of NFM. The adsorption responsive time to MO and MB, another key parameter of adsorbent, was showed in Fig. 4b&4d, respectively. PDA-$Co_{0.3}Ni_{0.7}Fe_2O_4@SiO_2$
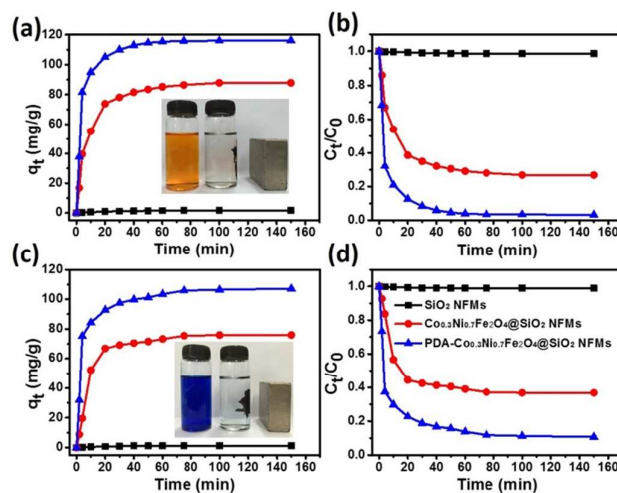
Fig.4 Time dependence of adsorption ability (a & c) and adsorption rate (b & d) of NFM template, NPs@NFM before and after dopamine coating in the 20 ppm MO (a & b) and MB solution (c & d).

NFMs could adsorb 92 wt% of MO and 80 wt% of MB in 30 min and achieve complete adsorption of MO and MB in 40 and 60 min, respectively. Compared with the literature results including carbon materials and polymer supported nanoparticles (Table S1), our NFMs have higher adsorption

capacities than most of adsorbents even at very low dye concentration i.e. low adsorption drive force. At the same time, the response time of NFMs is also competitive to those adsorbents. In addition, the PDA-$Co_{0.3}Ni_{0.7}Fe_2O_4$@SiO_2 NFM could be facilely recovered by an external magnet (insert of Fig. 4 a & c), which eliminates the tedious recycling process for regular adsorbents and also avoids secondary pollution. This feature is of great importance for real applications.

The adsorption kinetics of MB and MO on PDA-$Co_{0.3}Ni_{0.7}Fe_2O_4$@SiO_2 NFM were studied by two kinetic models including the pseudo-first-order and pseudo-second-order models. The models can be expressed as follows:

pseudo-first-order model

$$\ln(q_e - q_t) = lnq_e - k_{1t}$$

pseudo-second-order model

$$\frac{t}{q_t} = \frac{1}{k_2q_e^t} + \frac{t}{q_e}$$

where k_1 (min^{-1}) and k_2 (g/mg/min) are the rate constant of the pseudo-first-order and the pseudo-second-order, respectively, while q_e and q_t are the amounts of dye adsorbed (mg/g) at equilibrium and at time t (min). The adsorption rate constant can be determined from the plot of $\ln(q_e - q_t)$, t/q_t against t. The reliability of each kinetic model is tested by the fitness of the straight lines presented in Fig. S9 a & b. As to the pseudo-first-order model and pseudo-second-order model, the correlation coefficient are ($R^2 \geq 0.8909$ (MB) and 0.9014 (MO)) and ($R^2 \geq 0.9988$ (MB) and 0.9994 (MO)), respectively, illustrating the pseudo-second-order model is more suitable to describe the adsorption process of MO and MB onto PDA-$Co_{0.3}Ni_{0.7}Fe_2O_4$@SiO_2 NFMs.

Conclusions

In summary, we have successfully fabricated hierarchical PDA-$Co_{0.3}Ni_{0.7}Fe_2O_4$@SiO_2 NFMs, i.e. polydopamine protected metal oxides NPs supported on the electrospun SiO_2 NFMs. The prepared PDA-$Co_{0.3}Ni_{0.7}Fe_2O_4$@SiO_2 NFMs have fast response time, high adsorption capacity and affinity towards MO and MB. The electrospun SiO_2 NFM provides mechanical strength and easy accessible surface area required for adsorbent. The positively charged metal oxides NPs provide extra surface area for adsorption and high affinity towards negatively charged anionic dyes. The polydopamine coating provides adsorption affinity towards organic dyes as well as protection for NPs from leaching. The magnetism from the metal oxides NPs allows the easy recovery of the adsorbent, which prevents sorbent loss and secondary pollution. Therefore, the PDA-$Co_{0.3}Ni_{0.7}Fe_2O_4$@SiO_2 NFMs are expected to be a promising adsorbent for dye wastewater treatment and potential applications in catalysis, filtration, and other water remediation.

Notes and references

1   M. Purkait, S. DasGupta and S. De, *J Environ Manage*, 2005, **76**, 135.
2   J. Gong, J. Feng, J. Liu, Z. Jiang, X. Chen, E. Mijowska, X. Wen and T. Tang, *Chem Eng J*, 2014, **248**, 27.
3   J. Wang, L. Xu, Z. Zhang, P. Sun, M. Fang and H. Liu, *Rsc Adv*, 2015, **5**, 49696.
4   A. S. Franca, L. S. Oliveira and M. E. Ferreira, *Desalination*, 2009, **249**, 267.
5   Y. Tian, X. Wang and Y. Pan, *J. Hazard. Mater*, 2012, **213**, 361.
6   A. Liu, W. Zhou, K. Shen, J. Liu and X. Zhang, *Rsc Adv*, 2015, **22**, 17336.
7   H. Shi, L. Tan, Q. Du, X. Chen, L. Li, T. Liu, C. Fu, H. Liu and X. Meng, *Dalton T*, 2014, **43**, 12474.
8   Z. Jiang, J. Xie, D. Jiang, Z. Yan, J. Jing and D. Liu, *Appl Surf Sci*, 2014, **292**, 301.
9   N. Torad, M. Hu, S. Ishihara, H. Sukegawa, A. Belik, M. Imura, K. Ariga, Y Sakka and Y Yamauchi, *Small*, 2014, **10**, 2096.
10 X. Qian, T. Kamegawa, K. Mori, H. Li and H. Yamashita, *J Phys Chem C*, 2013, **117**, 19544.
11 C. Sprung and B. Weckhuysen, *J Am Chem Soc*, 2015, **137**, 1916.
12 L. Feng, M. Cao, X. Ma, Y. Zhu and C. Hu, *J. Hazard. Mater,* 2012, **217**, 439.
13 H. Ma, P. Williams and S. Diamond, *Environ Pollut*, 2013, **172**, 76-85.
14 Z. Favors, H. Bay, Z. Mutlu, K. Ahmed, R. Ionescu, R. Ye, O. Mihrimah and C. Ozkan, *Scientific reports*, 2015.
15 D. Xu, Z. Huang, R. Miao, Y. Bie, J. Yang, Y. Yao and S. Che, *J. Mater. Chem. A*, 2014, **2**, 19855.
16 Z. Zhang, C. Shao, Y. Sun, J. Mu, M. Zhang, P. Zhang, C. Zeng, P. Liang, C. Wang and Y. Liu. *J. Mater. Chem*, 2012, **22**, 1387.
17 L. Kong, X. Lu, X. Bian, W. Zhang and C. Wang, *Langmuir*, 2010, **26**, 5985.
18 J. He, W. Wang, F. Sun, W. Shi, D. Qi, K. Wang, R. Shi, F. Cui, C. Wang and X. Chen, *ACS nano*, 2015.
19 Y. Si, X. Tang, J. Ge, S. Yang, M El-Newehy, S. S. Al-Deyab, J Yu and B Ding, *Nanoscale*, 2014, **6**, 2102.
20 Y. Miao, R. Wang, D. Chen, Z. Liu and T. Liu, *Acs. Appl. Mater. Inter*, 2012, **4**, 5353.
21 R. Chen, W. Wang, X. Zhao, Y. Zhang, S. Wu and F. Li, *Chem. Eng. J,* 2014, **242**, 226.
22 X. Zhao, W. Wang, Y. Zhang, S. Wu, F. Li and J. Liu, *Chem. Eng. J*, 2014, **250**, 164.
23 Y. Si, X. Mao, H. Zheng, J. Yu, and B. Ding, *Rsc Adv.*, 2015, **5**, 6027.
24 Y. Si, C. Yan, F. Hong, J. Yu and B. Ding, *Chem Commun*. 2015.
25 S. K. Kailasa and H. F. Wu, *Analyst*, 2012, **137**, 1629.
26 J. Fu, Z. Chen, M. Wang, S. Liu, J. Zhang, J. Zhang, R. Han and Q. Xu, *Chem. Eng. J*, 2015, 259, 53.
27 C. Pan, R. Ding, Y. Hu and G. Yang, *Physica E*, 2013, **54**, 138.
28 N.Barakat, M.Khil, F. Sheikh and H.Kim, *J Phys Chem C*, 2008, **112**, 12225.
29 Barakat N. A, *J Mater Sci*, 2012, **47**, 6237.
30 S. Mikhailova, *J Struct Chem*, 2008, **49**, 206.
31 H. Zhu, R. Jiang, L. Xiao and W. Li, *J. Hazard. Mater*, 2010, **179**, 251.
32 H. Lee, S. Dellatore, W. Miller and P. Messersmith, *Science*, 2007, **318**, 426.
33 S. Zhang, Y. Zhang, G. Bi, J. Liu, Z. Wang, Q. Xu, H. Xu and X. Li, *J. Hazard. Mater,* 2014, **270**, 27.

Graphic abstract: